4176 Vol. 59, No. 13 / 1 May 2020 / Applied Optics Research Article

applied optics

Subaperture stitching interferometry based on the combination of the phase correlation and iterative gradient methods

Ruoyan Wang,[1] Zhishan Gao,[1] Dan Zhu,[1] Weijian Liu,[1] Wen Ji,[1] Zhenyan Guo,[1] Dasen Wang,[2] Lingjie Wang,[3] Yao Xu,[4] and Qun Yuan[1,*]

[1]School of Electronic and Optical Engineering, Nanjing University of Science and Technology, Nanjing 210094, China
[2]School of Mechanical Engineering, Nanjing University of Science and Technology, Nanjing 210094, China
[3]Key Laboratory of Optical System Advanced Manufacturing Technology, Changchun Institute of Optics, Fine Mechanics and Physics, Chinese Academy of Sciences, Changchun 130033, China
[4]Jiangsu Shuguang Opto-Electronics Co. Ltd., Yangzhou 225109, China
*Corresponding author: karmen86913@gmail.com

Received 20 January 2020; revised 27 March 2020; accepted 30 March 2020; posted 31 March 2020 (Doc. ID 388515); published 30 April 2020

Subaperture stitching interferometry (SAS) is an important method for map testing of large aperture optical components, in which a mechanical structure is often employed for the testing of each subaperture. By eliminating the phase deviation of the corresponding points in the overlapping regions of every adjacent subaperture, the whole aperture map can be obtained. Accurate subaperture positioning is an important guarantee for precise stitching. In this paper, a hybrid optimization algorithm is proposed to realize subpixel-level positioning accuracy in SAS based on the combination of the phase correlation and iterative gradient methods. The phase correlation method is adopted to calculate the pixel-level positioning deviation first, and the subpixel deviation is derived and then corrected by iterative optimization through the gradient method. The subpixel-level positioning accuracy of the proposed optimization algorithm is verified by simulations and a 76.2 mm off-axis parabolic mirror is chosen as an experimental testing sample. The surface map obtained from the proposed hybrid optimization method is consistent with the full aperture testing result, which also verifies that the proposed optimization algorithm is a powerful tool with subpixel-level positioning accuracy in SAS testing.

https://doi.org/10.1364/AO.388515

1. INTRODUCTION

Interferometry is a non-contact technology for acquiring the surface information of the testing components with high accuracy, and it is widely used in industrial, medical, and astronomical applications [1]. With the increasing demand of large-aperture optical systems in various fields, suitable testing methods are necessary considering both accuracy and economic factors. The traditional method is to test the full size of the large-aperture components directly with the help of the corresponding large interferometer. Although this method facilitates the measurement process, large interferometers are expensive and difficult to manufacture. Instead, subaperture stitching interferometry (SAS) can be used to obtain the full surface map of large-aperture components without the need of large interferometers. The SAS testing method was firstly proposed by Kim in 1982 [2]. The full aperture of the tested components is divided into several subapertures, each subaperture is tested, and the surface maps of all the subapertures are then stitched to obtain the full aperture map. SAS testing is now widely used for surface map testing of large-aperture optics and aspherical optics, and SAS systems show excellent performance in testing of large-aperture plane mirrors and moderate aspheric optical components [3–5].

The surface map obtained from SAS testing is described by the phase information of the discrete points in each subaperture. The surface map of each subaperture contains not only the figure of the tested components but also the reference surface shape error, alignment error, and positioning error. The quality of the transmission flat or sphere is so high that the reference surface shape error can be ignored. The alignment error induced by tip, tilt, and defocus is corrected by the least-squares (LS) method. The positioning error, introduced mainly by the mechanical scanning of each subaperture, will cause a mismatch of the corresponding points in the overlapping regions of two adjacent subapertures, which severely decreases the testing accuracy.

In order to improve the positioning accuracy or eliminate the positioning error as much as possible, a simple and effective method is to use a high-precision translation stage to realize the subaperture scanning. However, this method will greatly increase the testing expense. Therefore, some measures for assistant positioning were proposed in cases where the mechanical positioning accuracy is not very high. The marker point method proposed by Maurer realized the subaperture testing data match by aligning the positions of the marker points, which are artificially marked in the sample [6]. The stereoscopic method introduced by Zhang uses two cameras to simultaneously image the marker points on the mechanical motion device, and then calculates the position of the markers to position the subaperture [7]. In addition, there were some algorithms proposed to retrieve the positioning error. Tang proposed a method that considered the six freedom degrees of rigid body motion and obtained the optimal estimation of positioning error by fitting the phase deviation of the overlapping regions [8]. Sjöedahl proposed an iterative algorithm to calculate the optimal estimate of the six degrees of freedom, updating the overlapping region until the algorithm converges to a certain precision [9]. Chen transformed the subaperture data to a three-dimensional global coordinate system and optimized the poses between the subapertures and corresponding point pairs of the overlapping regions [10]. QED Technologies proposed a slope-based algorithm to compensate for the positioning error by the using the slope of the surface error [11]. In this method, the compensation factors are highly dependent on the coincidence degree between the sample points from two subapertures in the overlapping region, which means even small sample dislocation, usually observed in actual experiments, will decrease the stitching accuracy and robustness.

The positioning deviation is defined as the actual position deviated from the nominal value, which can be divided into the integer-pixel-level and subpixel-level positioning deviations. The subpixel-level positioning accuracy is of great importance for SAS testing, which is based on the elimination of the integer-pixel-level and subpixel-level positioning deviations. We propose a hybrid optimization algorithm to realize subpixel positioning accuracy in SAS based on the phase correlation and iterative gradient method without sacrificing the computing time too much. The phase correlation and gradient-based iterative optimizations are leveraged to estimate the integer-pixel-level and subpixel-level positioning deviations, respectively. The phase correlation method can obtain the integer-pixel-level deviation between subapertures with high efficiency and accuracy, and the gradient method performs more precisely in subpixel positioning. Moreover, the measures to deal with the interactions between the alignment error and the positioning error are considered.

In this paper, the principle and procedure of the proposed algorithm are elaborated in Section 2. The feasibility of our algorithm is validated by simulations in Section 3. The proposed algorithm is applied for testing a 76.2 mm off-axis parabolic mirror in Section 4. Discussions are presented in Section 5.

2. PRINCIPLE

In order to realize SAS, all subapertures defined in their local coordinate systems need to be placed in a uniform global coordinate system after alignment error correction by the LS method. As shown in Fig. 1, two adjacent subapertures w_1 and w_2 are taken as an example. The subaperture illustrated by the orange dotted line is the ideal position of w_2, and u_0 and v_0 are its relative translations in the x and y directions from w_1, which equal to the nominal displacement value of the translation stage. However, positioning errors of the translation stage are unavoidable. The actual position of subaperture w_2 is illustrated by the orange circle, in which (u, v) and (du, dv) are the integer pixel and subpixel deviation between the ideal and actual positions, respectively. In the global coordinate system, the overlapping regions w_{22} can be obtained by shifting w_{11} by $(u + du, v + dv)$, which can be expressed as $w_{11}(x, y) = w_{22}(x + u + du, y + v + dv)$.

The overlapping areas from the two adjacent subapertures are specified as $w_1 1$ and $w_2 2$, respectively, which correspond to the same area in the surface under test. Therefore, they are not matched in the global coordinate system as shown in Fig. 1(a), where w_1 and w_2 are placed according to their nominal relative positions (u_0, v_0). With known positioning deviations $(u + du, v + dv)$, w_{11} and w_{22} are well matched as illustrated in Fig. 1(b), and thus precise stitching can be executed. The accurate solving of positioning deviations is the determinant factor, and it is elaborated in the next sections. The positioning deviations are divided into integer-pixel level and subpixel level and then eliminated by the following methods.

A. Integer-Pixel Positioning Deviation Elimination Based on Phase Correlation

In order to eliminating the integer-pixel-level deviation, the global search method is generally used to obtain the relative position between the two subapertures. Global searching [12] can achieve accurate positioning, but it is time-consuming, and the searching range needs to be preset based on the estimation of the positioning deviation. To overcome these disadvantages, the phase correlation method is applied for fast and accurate positioning in the integer-pixel level. The choice of the phase correlation method used for the integer-pixel positioning in our study is mainly motivated by the acceleration of the

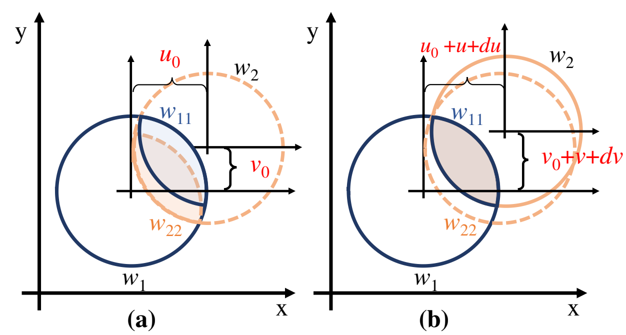

Fig. 1. Stitching model of two adjacent subapertures in the global coordinate system: blue circle represents subaperture w_1, and the orange dotted circle represents the ideal position of another subaperture w_2 with the relative translation (u_0, v_0) in the x and y directions from w_1. The actual position of w_2 is illustrated as the orange circle, which has a positioning deviation $(u + du, v + dv)$ from its ideal position in the x and y directions.

integer-pixel positioning and robustness of its performance without a previous estimation of the deviation.

The phase correlation method [13] is used to eliminate the deviation between two subapertures in the integer-pixel level to get the values of u and v. The basic idea of this method is based on the translational property of the Fourier transform. The relative motion of the image in the spatial domain will only cause a linear change of phase in the frequency domain, while the amplitude of the spectrum does not change.

Two squares w_1' and w_2', with the same size $n \times n$, are selected from the overlapping regions w_{11} and w_{22}, respectively. As mentioned above, ignoring the subpixel-level positioning deviation, the deviation of w_1' and w_2' can be expressed as

$$w_1'(x, y) = w_2'(x + u, y + v). \quad \textbf{(1)}$$

Through taking the Fourier transform of surface data in the overlapping regions, we can get

$$W_1(p, q) = W_2(p, q) \cdot e^{-i \cdot 2\pi(u \cdot p + v \cdot q)}, \quad \textbf{(2)}$$

where $W_1(p, q)$ and $W_2(p, q)$ are the Fourier transform of $w_1'(x, y)$ and $w_2'(x + u, y + v)$, and (p, q) is the coordinate in the frequency domain.

The cross-power spectrum of the two subapertures can be calculated in the form

$$H(p, q) = \frac{W_1 \cdot W^*{}_2}{|W_1| * |W_2|} e^{-i \cdot 2\pi(u \cdot p + v \cdot q)}. \quad \textbf{(3)}$$

The inverse Fourier transform is performed, and the integer-pixel-level deviation $(u, \ v)$ is obtained by detecting the peak coordinates of the phase correlation function.

B. Subpixel Positioning Deviation Elimination Based on the Iterative Gradient Method

The position adjustment of the two subapertures in the global coordinate system was performed according to the integer pixel deviation obtained in Section 2.A. In this way, the tilt and defocus of the subapertures with respect to the standard transmission flat are different from each other, so the LS method is used again to eliminate the alignment error. In addition, the subpixel positioning deviation results in a mismatch of overlapping regions in different subapertures. Therefore, the subpixel-level positioning is required to make the corresponding points coincident for a better stitching result.

In order to obtain the deviation in the subpixel level, a simple approach is grid searching [14]. First, we obtain the upsampling surface data by interpolation, and then the grid search method is employed to find the position with the highest coincidence. Although grid searching can obtain a relatively accurate positioning deviation, it ignores the interaction between the positioning error and the relative alignment error. Therefore, in this section, an iterative solution based on the gradient of the correlation function for the subpixel-level position is proposed. By alternately optimizing the relative alignment error and subpixel positioning deviation of the two adjacent subapertures, the uniformity of the overlapping regions is improved, and the accurate positioning of the two subapertures is realized for more accurate surface map testing. Through iteration, the accuracy of the deviation elimination is ensured, and mutual influence between the positioning deviation and alignment error is better suppressed.

For the two subapertures in the current positions, the relative alignment errors are first optimized by the LS method. The relative tilt and defocus between the two subapertures are calculated and eliminated. Then we choose the square of the normalized covariance function as the correlation function. By using the gradient of the correlation function, the subpixel positioning deviation can be solved.

Assume that the overlapping regions of the two subapertures after integer-pixel-level positioning are $w_1''(x, \ y)$ and $w_2''(x + du, \ y + dv)$, and the Taylor expansion is performed for w_2'' as

$$\begin{aligned} w_2''(x + du, y + dv) &= w_2''(x, y) + du \cdot w_{2u}''(x, y) + dv \cdot w_{2v}''(x, y) \\ &+ \frac{1}{2}(du)^2 \cdot w_{2uu}''(x, y) + du \cdot dv \cdot w_{2uv}''(x, y) \\ &+ \frac{1}{2}(dv)^2 \cdot w_{2vv}''(x, y). \end{aligned} \quad \textbf{(4)}$$

$\prod$ is the correction function, and in this paper it is defined as [15]

$$\prod = \frac{\left[\sum_{i=1}^n \sum_{j=1}^n \left[w_1''(x_i, y_j) - \overline{w_1''}\right] \cdot \left[w_2''(x_i + du, y_j + dv) - \overline{w_2''}\right]\right]^2}{\sum_{i=1}^n \sum_{j=1}^n \left[w_1''(x_i, y_j) - \overline{w_1''}\right]^2 \cdot \sum_{i=1}^n \sum_{j=1}^n \left[w_2''(x_i + du, y_j + dv) - \overline{w_2''}\right]^2}, \quad \textbf{(5)}$$

where $\overline{w_1''}$ and $\overline{w_2''}$ are the average values of the surface data of w_1'' and w_2'', respectively. The positioning deviations du and dv satisfy the condition that $\frac{\partial \prod}{\partial du} = 0$ and $\frac{\partial \prod}{\partial dv} = 0$.

The position of the two subapertures in the global coordinate system is adjusted according to the subpixel error $(du, \ dv)$. The value of $w_2''(x + du, \ y + dv)$ corresponding to the integer pixel point of $w_1''(x, \ y)$ is obtained by cubic interpolation. A new relative alignment error is generated between the repositioned subapertures. The process of eliminating the relative alignment error and subpixel-level positioning in the above is repeated until the positioning deviation satisfies the stop criterion (du & $dv < 0.001$).

C. Implementation Steps of the Proposed Hybrid Optimization Algorithm

The flowchart of our proposed hybrid optimization algorithm is illustrated in Fig. 2, and the specific implementation steps can be described as follows:

(1) Select two adjacent subapertures w_1 and w_2.
(2) Estimate the relative alignment error between w_1 and w_2 using the LS method.

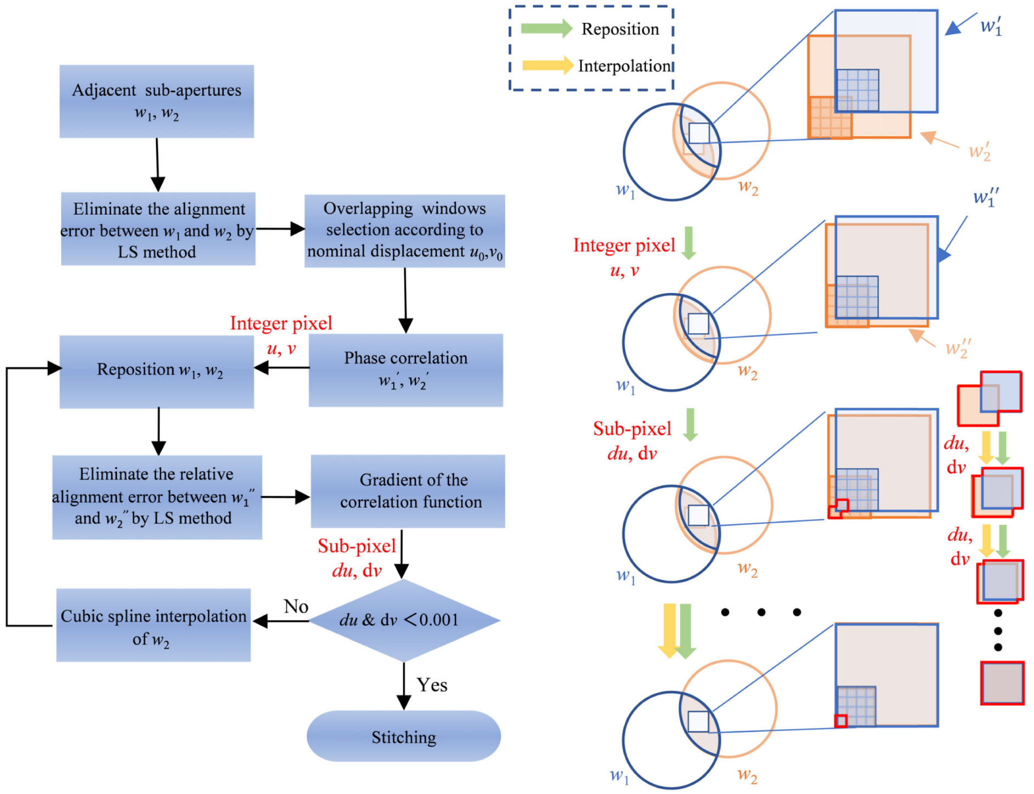

Fig. 2. Flowchart of the proposed hybrid optimization algorithm.

(3) Select two square windows w_1' and w_2' in the overlapping region of the subapertures according to the nominal relative displacement values u_0 and v_0 between w_1 and w_2.
(4) Get the integer-pixel-level positioning deviation (u, v) in the x and y directions based on the phase correlation method.
(5) Reposition w_1 and w_2 in terms of the obtained (u, v). The two square windows w_1' and w_2' in the overlapping regions after integer-pixel-level repositioning are expressed as w_1'' and w_2''.
(6) Employ the LS method again to eliminate the relative alignment error between w_1'' and w_2''.
(7) Calculate the gradient of the correlation function to eliminate the subpixel-level deviation (du, dv), and further adjust of the positions between the two subapertures w_1 and w_2 by keeping w_1 fixed.
(8) If the obtained du and dv are both smaller than 0.001, then go to step 10; if not, go to step 9.
(9) Perform cubic spline interpolation of the initial surface data of subaperture w_2 to get the surface data of w_2'' at the updated pixel positions and repeat steps 5 to 8.
(10) Stitch the two subapertures w_1 and w_2.

3. SIMULATION ANALYSIS

The proposed hybrid optimization algorithm was first validated on two simulated adjacent subapertures. The surface data of a spherical mirror acquired by a 101.6 mm aperture Zygo interferometer was used as the original data of the overlapping area, which is shown in Fig. 3(a). The selection of the overlapping region is illustrated in Fig. 3(b), where the gray circle represents the original surface data, and subaperture w_1 and

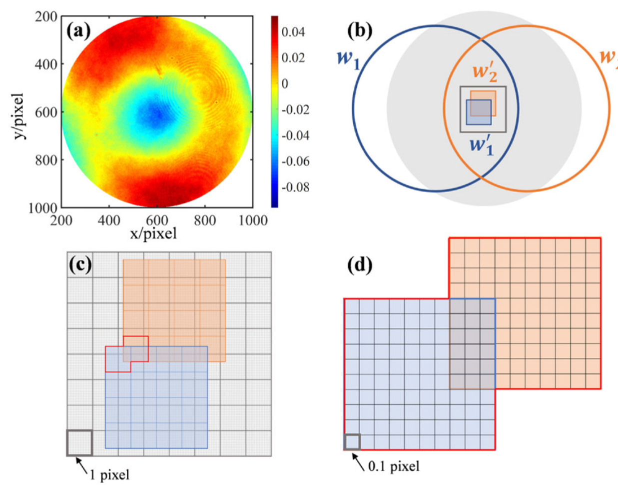

Fig. 3. Schematic diagram of the simulated subpixel positioning deviation between two adjacent subapertures. (a) Surface map of spherical mirror acquired by a 101.6 mm Zygo interferometer. (b) Selection of the overlapping regions. In (c), gray squares are part of the original surface data obtained from the interferometer, and one grid corresponds to one pixel in the CCD target. The blue squares and the orange ones are parts of the overlapping region in the two adjacent subapertures. (d) Enlarged version of the red block in (a); each small square in it represents 0.1 pixel before interpolation, and the surface data of whole blue square is the mean of all the 10 × 10 small square data.

subaperture w_2 are represented by the blue and orange circles, respectively. A square matrix in the overlapping region of each subaperture was chosen for the following simulation.

To show the positioning deviation between the two subapertures, the overlapping regions were described as Fig. 3(c), in which one small square represented one pixel in the original matrix. To simulate the subpixel-level positioning deviation, the cubic spline interpolation was applied to the original data. We assumed the size of original matrix is $M \times M$ pixels, and then after interpolation, the high-resolution surface matrix was $10M \times 10M$ pixels. Next, two adjacent $N \times N$ pixels′ ($N < 10M$) subapertures were selected form the high-resolution surface matrix; the overlapping regions are shown as the blue and orange grids in Fig. 3(c). Here the positioning error and the alignment error caused by tilt, defocus, and axial translation were added to subaperture w_2 manually. The positioning deviation introduced is (7, 34) pixels in the x and y directions in the matrix after interpolation as shown in Fig. 3(d). We applied the 10th downsampling-average method to realize the simulation of subpixel positioning deviation by downsampling the $N \times N$ pixels′ surface map matrix to an $n \times n$ pixels low-resolution target, where n equals to $N/10$. In our simulation, the size N of the overlapping region after interpolation was set as 2000, and after the 10th downsampling-average method, the matrix was 200×200 pixels. For each pixel we calculated the intensity value by averaging the corresponding 10 pixels in the original surface map. Therefore, the positioning deviation changed from (7, 34) pixels to (0.7, 3.4) pixels.

After the introduction of the subpixel-level positioning error, we applied the proposed method to estimate the positioning deviation. The phase correlation method was first used to calculate the pixel-level positioning deviation between the two subapertures in the same coordinate. As shown in Fig. 4(a), the Dirac function was calculated, and then the integer pixel deviation between the two subapertures was (1, 3) pixels, by finding the coordinates of the peak.

According to the deviation of the two subapertures, their coordinate positions were adjusted to make a better overlap. Then the iterative correlation function gradient method was applied to estimate the subpixel deviation between the two subapertures, and the deviations during the iteration process are shown in Fig. 4(b). After 10 iterations, the estimated deviations were (−0.3043, 0.4036) pixels in the x and y directions. Combined with the integer deviation, the positioning deviation calculated by our proposed optimization algorithm is (0.6957, 3.4036) pixels, which is highly consistent with the simulated deviation (0.7, 3.4) pixels. This high-accuracy positioning is achieved within $3 \sim 5$ iterations as shown in Fig. 4(b), and it demonstrates that the proposed method is still efficient although an iteration procedure is necessary.

By estimating the positioning deviation with high accuracy, the residual phase difference between overlapping regions w_1'' and w_2'' will be greatly reduced. We compared the residual phase difference only after integer pixel correction with that after our subpixel level elimination. The results are shown in Fig. 5.

The RMS values of the two method are $1.25 \times 10^{-3}\,\lambda$ and $2.21 \times 10^{-4}\,\lambda$, corresponding to 8.6% and 1.5% of the original surface data w_1'', which demonstrates that the positioning

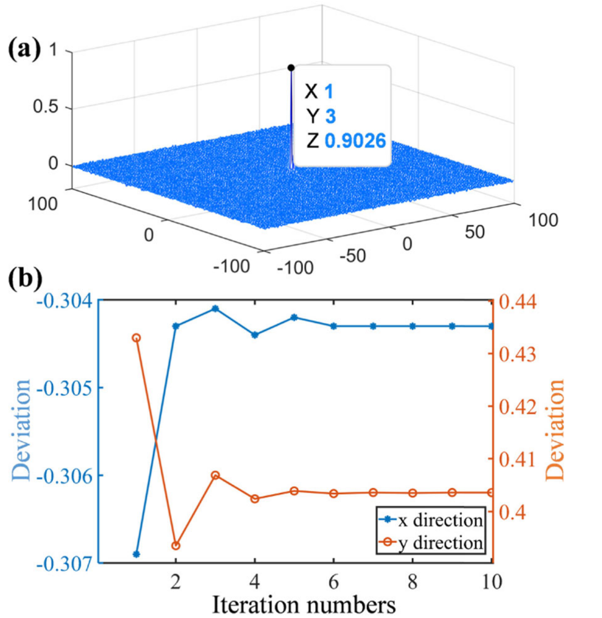

Fig. 4. Deviations estimated from the proposed algorithm. (a) Peak of the Dirac function for integer-pixel-level deviation estimation. (b) Subpixel-level deviations in the x and y directions during the correction process.

accuracy is much higher after subpixel positioning, and which also improves the surface map testing accuracy.

The correlation-function-based gradient method is one of the meaningful subpixel positioning methods. However, when the deviation between the initial position and the actual position is too large, the positioning is not accurate enough. Meanwhile, considering the mutual influence of the positioning error and alignment error, the iterative gradient method was adopted to solve the two problems at the same time.

In order to verify that the positioning accuracy of our iterative gradient method is higher than that of the single-gradient

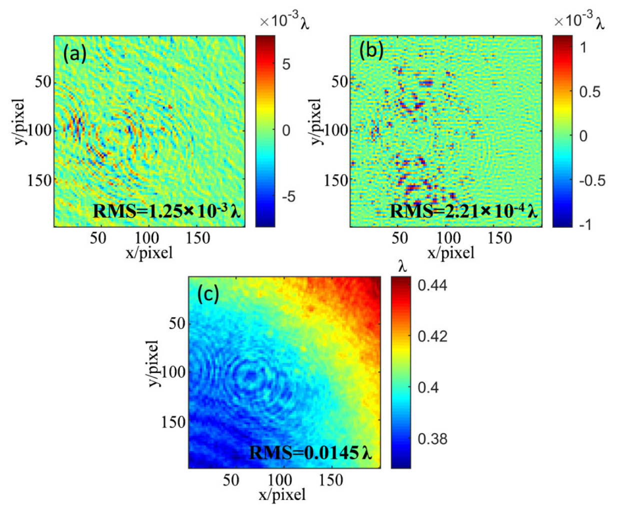

Fig. 5. (a) Residual map between the deviation-correction surface map w_2'' (b) only after integer pixel repositioning and (c) after subpixel-level elimination by our proposed method and surface map w_1''.

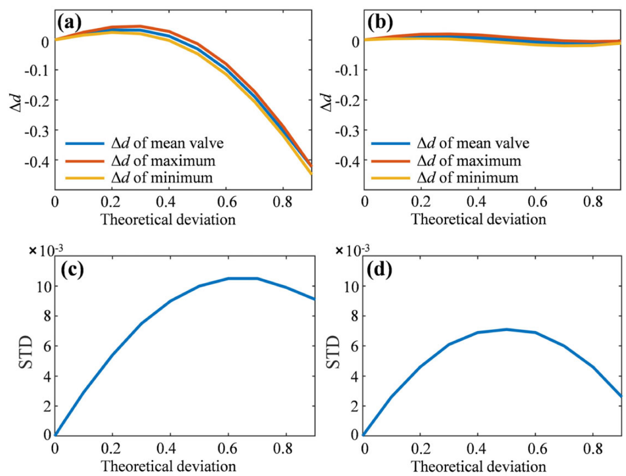

Fig. 6. Statistical results of the difference (Δd) and standard deviation (STD) between the estimated theoretical deviation and the deviations from different method: (a) and (c) were obtained from the single-gradient method; (b) and (d) were from the proposed iterative gradient method.

method, we randomly selected 100 overlapping regions of the two subapertures in the original surface map, and the size of the selected region was 200×200 pixels. For each region, by interpolation and the downsamping-average method, we introduced 0.1, 0.2, … 0.8, and 0.9 pixel deviation of the two subapertures in the x or y direction. Then the single-gradient method and our iterative gradient method were adopted to estimate the positioning error. The statistical results of the 100 random regions are shown in Fig. 6, in which the x axis is the theoretical deviation and the y axis is the difference between the estimated and the introduced deviation.

From Fig. 6(a), we found that for the single-gradient method, the positioning accuracy is within 0.1 pixel when the introduced deviation is smaller than 0.5 pixel. For 0.5 pixel introduced deviation, the maximum absolute error between the estimated and actual results is 0.0463 pixel. For the introduced deviation larger than 0.5 pixel, the single-gradient method cannot give accurate positioning deviation. But for the iterative gradient method, according to the last positioning result, the points of the overlapping regions were corresponded one-to-one by interpolation, and the relative alignment error between the two subapertures was eliminated by the LS method. Then the positioning deviation after alignment was further obtained by the correlation function gradient method. Accurate results were acquired after multiple iterations. The positioning results in Fig. 6(b) show that when the theoretical deviation is 0.3 pixel, the positioning difference between estimated and introduced deviation is the largest, with a deviation of 0.0196 pixel, which verifies that the positioning accuracy of the iterative algorithm is significantly higher than that of the single-gradient method. The standard deviations (STD) of the single-gradient and iterative gradient methods are shown in Figs. 6(c) and 6(d); the STD of the iterative positioning algorithm is much smaller, which means a better stability.

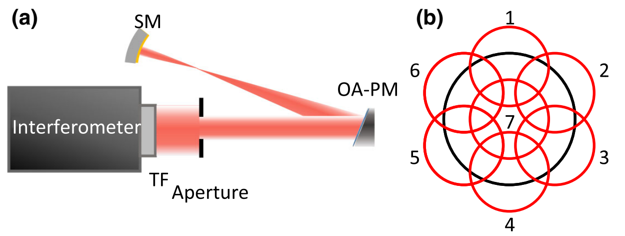

Fig. 7. (a) Schematic of off-axis parabolic mirror SAS testing. TF, flat transmission flat; OA-PM, tested off-axis parabolic mirror; SM, spherical mirror. (b) Layout of seven subapertures.

4. EXPERIMENTAL RESULTS

In order to verify the feasibility of the proposed hybrid optimization algorithm a 76.2 mm off-axis parabolic mirror was tested by an interferometer working at 632.8 nm from Zygo Inc. Since the diameter of the interferometer used is 100 mm, which is larger than the full aperture of the tested off-axis parabolic mirror, a 50 mm iris is placed at the exit of the interferometer to imitate a small-diameter interferometer testing a large-diameter mirror. The overall optical path follows the self-collimation method. As shown in Fig. 7(a), the parallel light beam from interferometer is incident on the off-axis parabolic mirror, and the beam is reflected by the spherical mirror and returns along the incident path.

As shown in Fig. 7(b), the off-axis parabolic mirror (shown in a black circle) is divided into seven subapertures (red circles), and a five-dimensional mechanism is employed to move the tested mirror to realize the testing of the seven subapertures, which is shown in Fig. 8. The original interference fringes of the subapertures are shown in Fig. 8(a), and the corresponding surface maps after eliminating the tilt and defocus are shown in Fig. 8(b).

Using the subpixel-level positioning error estimation algorithm proposed in this paper, the positioning errors between subapertures are eliminated, and the full-aperture surface map obtained by stitching is shown in Fig. 9(b), in which the peaks and valleys (PV) is $2.6223\,\lambda$ and RMS is $0.3523\,\lambda$. The surface map obtained from full-aperture direct testing by Zygo interferometer is illustrated in Fig. 9(a), while $\mathrm{PV} = 2.658\,\lambda$ and $\mathrm{RMS} = 0.352\,\lambda$. The residual error of the SAS testing and full-aperture direct testing is shown in Fig. 9(d), the PV value is $0.182\,\lambda$ and RMS value is $0.013\,\lambda$. Then we compared our method with the traditional LS method. The surface map shown in Figs. 9(c) and 9(e) is the residual error between the surface map recovered from the traditional LS method and the full-aperture direct test result. The PV value and RMS of the proposed method are both smaller than those of LS method, which means that by the proposed method, the positioning error is eliminated precisely, and surface map is more coincident with the full-aperture direct testing result.

5. DISCUSSION

In this paper, a hybrid optimization algorithm is proposed to eliminate the positioning deviation in SAS testing up to the subpixel level. The phase correlation method is used to estimate

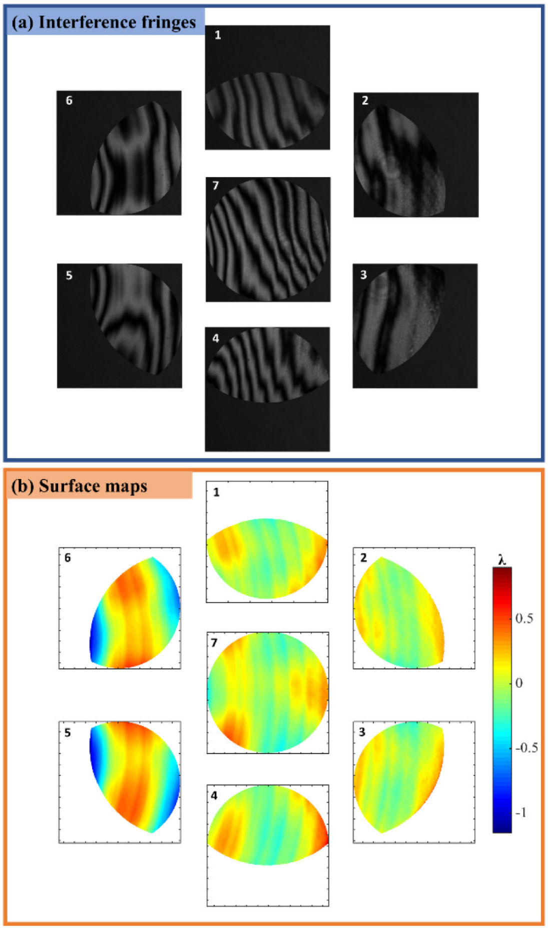

Fig. 8. Subaperture stitching testing of 76.2 mm off-axis parabolic mirror experimentally. (a) Original interference fringes; (b) surface maps of the all subapertures after eliminating the tilt and defocus.

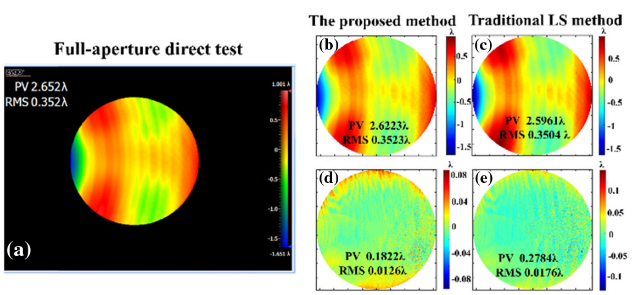

Fig. 9. Experimental results of the tested parabolic mirror. (a) Surface map of SAS testing with subpixel-level positioning deviation eliminated; (b) surface map from full-aperture direct testing; (c) residual error between the surface maps in (a) and (b).

the positioning deviation at the integer-pixel level. For subpixel-level deviation, the iterative correlation function gradient method is employed to improve the positioning accuracy and get a more accurate surface map of the tested components. Meanwhile, the iterative gradient method effectively solved the problem of mutual interference between positioning error and alignment error. The positioning accuracy of the proposed method is 0.02 pixel. The difference between the integer-pixel stitching and sub-pixel stitching is compared by simulations. The SAS testing after eliminating the subpixel-level positioning errors shows better performance both in simulated and experimental results, which is much more coincident with the result of full-aperture direct testing.

Funding. National Natural Science Foundation of China (U1931120, 61701239); Key Technologies Research and Development Program (2019YFB2005500); Fundamental Research Funds for the Central Universities (30917011107, 30918014115-004); Chinese Academy of Sciences (KLOMT190201).

Disclosures. The authors declare that there are no conflicts of interest related to this paper.

REFERENCES

1. D. Malacara, ed., *Optical Shop Testing* (Wiley, 2007), Vol. **59**.
2. C. J. Kin and J. C. Wyant, "Subaperture test of a large flat or a fast aspheric surface," J. Opt. Soc. Am. **71**, 1587 (1981).
3. C. Zhao, R. A. Sprowl, M. Bray, and J. H. Burge, "Figure measurement of a large optical flat with a Fizeau interferometer and stitching technique," Proc. SPIE **6293**, 62930k (2006).
4. L. Yan, X. Wang, L. Zheng, X. Zeng, H. Hu, and X. Zhang, "Experimental study on subaperture testing with iterative triangulation algorithm," Opt. Express **21**, 22628–22644 (2013).
5. J. Fleig, P. Dumas, P. E. Murphy, and G. W. Forbes, "An automated subapeture stitching interferometer workstation for spherical and aspherical surfaces," Proc. SPIE **5188**, 296–307 (2003).
6. R. Maurer, F. Schneider, C. Vogt, M. Schinhaerl, P. Sperber, and R. Rascher, "Physical marker based stitching process of circular and non-circular interferograms," Proc. SPIE **8083**, 80830Q (2011).
7. P. Zhang, H. Zhao, X. Zhou, and J. Li, "Sub-aperture stitching interferometry using stereovision positioning technique," Opt. Express **18**, 15216–15222 (2010).
8. S. Tang and C. Brian, "Measuring height variation over entire wafer surface with high lateral resolution," Proc. SPIE **6672**, 667209 (2007).
9. M. Sjöedahl and B. F. Oreb, "Stitching interferometric measurement data for inspection of large optical components," Opt. Eng. **41**, 403–408 (2002).
10. S. Y. Chen, S. Y. Li, and Y. F. Dai, "Iterative algorithm for subaperture stitching interferometry for general surfaces," J. Opt. Soc. Am. A **22**, 1929–1936 (2005).
11. D. Golini, G. Forbes, and P. Murphy, "Method for self-calibrated sub-aperture stitching for surface figure measurement," U.S. patent 6,956,657 B2 (18 October 2005).
12. Y. Chen, E. Miao, Y. Sui, and H. Yang, "Modified sub-aperture stitching algorithm using image sharpening and particle swarm optimization," J. Opt. Soc. Korea **18**, 341–344 (2014).
13. C. D. Kuglin and D. C. Hines, "The phase correlation image alignment method," in *Proceedings of the International Conference of the Cybernetics Society* (1975), pp. 163–165.
14. L. Yan, X. Wang, L. Zheng, X. Zeng, H. Hu, and X. Zhang, "Experimental study on subaperture testing with iterative triangulation algorithm," Opt. Express **21**, 22628–22644 (2013).
15. J. Zhang, G. Jin, S. Ma, and L. Meng, "Application of an improved subpixel registration algorithm on digital speckle correction measurement," Opt. Laser. Technol. **35**, 533–543 (2003).